

## N719-Dye Based Electrochemical Light and Temperature Sensor

Asma Khalil<sup>1,2</sup>, Zubair Ahmad<sup>3\*</sup>, Farid Touati<sup>1</sup> and Mohamed Masmoudi<sup>2</sup>

<sup>1</sup> Department of Electrical Engineering, Qatar University, 2713, Doha Qatar

<sup>2</sup> Department of Electrical Engineering, National Engineering School of Sfax, Sfax 3038, Tunisia

<sup>3</sup> Center for Advanced Materials (CAM), Qatar University, 2713, Doha Qatar

\*E-mail; [zubairtarar@qu.edu.qa](mailto:zubairtarar@qu.edu.qa)

Received: 2 September 2019 / Accepted: 22 October 2019 / Published: 30 November 2019

---

In this article, electrochemical N719-Dye based integrated light and temperature sensors have been reported. The fabricated sensor exhibits interesting features such as low cost, simple fabrication process, high sensitivity and self-powering capability. Current-Voltage (I-V) and Electrochemical Impedance Spectroscopy (EIS) characterizations have been performed to study the electrical and photo-electrochemical response of the sensors. The electrochemical response has been investigated as a function of incident light intensity and temperature. The sensors show a linear current-irradiance and current-temperature relationships. The transient response and recovery times of the photo sensors are 220 msec and 630 msec, respectively. The measured sensor's responsivity is  $3 \times 10^{-4}$  A/W while its sensitivity is  $7 \mu\text{S.m.W}^{-1}$ . The above results make the newly proposed integrated light and temperature sensor very promising and pave the way for the development of simple and cost effective light and temperature sensors.

---

**Keywords:** Electrochemical cell, Dye Sensitized Solar Cell, Light sensor, Temperature sensor, electrochemical Impedance Spectroscopy.

### 1. INTRODUCTION

Electrochemical sensors are the versatile components used in indoor, outdoor applications and play a pivotal role in security, agriculture and food safety [1, 2]. Sensors are usually associated to other automated devices for monitoring and helping in decision-making. Light and temperature sensors, in particular, have a very wide range of applications. Light sensors are used in light level sensing, digital imaging and object detection. While the temperature sensors are used for heat changes detection in harsh environment and self-heating of electronic devices such as integrated circuits (ICs) and biomedical devices. A typical electrochemical sensor structure consists of a reference electrode and a

sensing electrode separated by an electrolyte. This configuration reminds the structure and the working principles of the Dye Sensitized Solar Cell (DSSC). DSSC origins starts with the history of semiconductor sensitization. It is in fact a result of the convergence of photo-electrochemistry and photography, which rely on photo-induced charge separation at a solid-liquid interface [3].

The operating mechanism of the DSSC has been reported in several works in the literature [4-7]. Initially, dye molecules are attached to the mesoporous semiconducting TiO<sub>2</sub> surface. When a light photon hits the cell surface, electrons are generated from the excited dye molecules and injected into the TiO<sub>2</sub> conduction band. The electrons then hop and reach the FTO electrode. DSSC has several advantages and it is well known for being safe and reliable. Besides, it can be produced on thin, flexible and lightweight substrates. This type of devices is aesthetically attractive, relatively inexpensive and simply fabricated with ecologically friendly and non-toxic materials.

N719 dye is the most popular benchmark used for DSSC fabrication [8]. N719 is a good choice for thermally stable devices as well. Although the DSSC efficiency remains low compared to its counterparts, its application can be extended to promising sensors applications [9, 10]. The current study has been inspired from the several aged and stabilized electrochemical N719-Dye based solar cell samples. Although the aging process of the cells results into a low photocurrent, however, the current remains enough for the sensing application. Since sensors operation is based on the sensitivity, therefore, the low efficiency of DSSC is not anymore a drawback for the sensors. A few researches have already reported some sensor applications based on DSSC structure [11]. Shikoh, [12] fabricated a bulk heterojunction thin film/liquid electrolyte based electrochemical sensor for visible light detection. Qadir [13] have developed a binary blend based DSSC photo sensor using PCPDTBT and MEH-PPV composite as light sensitizer. Also, in 2011, Texas Instrument declared the DSSC to be a better candidate photovoltaic under indoor conditions [14]. These valuable properties of energy harvesting under low lighting levels make the DSSC an excellent choice for photo sensor application. Additionally, the thermal properties and the stability of the used N719 dye added values to the device and broaden the application to an electrochemical based light and temperature integrated sensor. The aim of this work is to demonstrate the prospective applications of an N719dye based electrochemical light and temperature sensors.

## 2. EXPERIMENTAL

The sensor samples have been fabricated in the lab environment using the N719 dye. The fabrication process starts with the photo electrode fabrication followed by the electrode sensitization and device assembly. TiO<sub>2</sub> paste from Solaronix has been deposited as a thin layer on the ITO substrates using doctor blade technique. After deposition, the paste was left to dry in ambient air. TiO<sub>2</sub> films have been then sintered at 450 °C for 60 minutes. The obtained thickness was ~15µm. For the TiO<sub>2</sub> coated ITO photo electrode sensitization, the TiO<sub>2</sub> pre-coated glass electrode slides have been placed into a glass container, and completely submerged with the N719 dye and allowed to soak overnight to let the infiltration and absorption of the dye molecules into the mesoporous TiO<sub>2</sub> layer. After the 24h, the electrodes were taken out and carefully rinsed with acetone and left to dry for 30 minutes in ambient air. The electrodes were then joined and sealed to an ITO/Platinum-based counter

electrode using a polymeric surlyn film and the assembly has been heated at 100°C for few seconds to form an effective sealing. The redox system iodide/tri-iodide ( $I/I_3^-$ ) has been dissolved in an organic solvent and injected through a drilled hole using a vacuum syringe in the vacant space between the two electrodes. Finally, to avoid electrolyte leakage, the edges and the injection holes have been sealed using a sealant and a thin glass slab. Finally, the resulting obtained device is composed of ITO/TiO<sub>2</sub>/N719-Dye/Pt Electrode layers. Figure 1 illustrates in details the structure and the configuration of the fabricated device. The electrons flow and energy bands is illustrated in Figure 2.

The optical and thermal study has been conducted on six DSSC samples that have been left to open indoor conditions for few months after fabrication, the cells are then very well stabilized. The focus of this study is oriented to sensor sensitivity towards light and temperature. The I-V characteristic measurements have been carried out using a KEITHLY 4200 Source Meter associated with a Xenon Solar Simulator under different irradiances. The intensity of the solar simulator has been varied over the range of 110- 1000 mW/cm<sup>2</sup>, and the voltage has been swept from 0 to 1V. The temperature dependence study has been performed in the temperature range of 30°C to 85 °C with a step of 5°C.

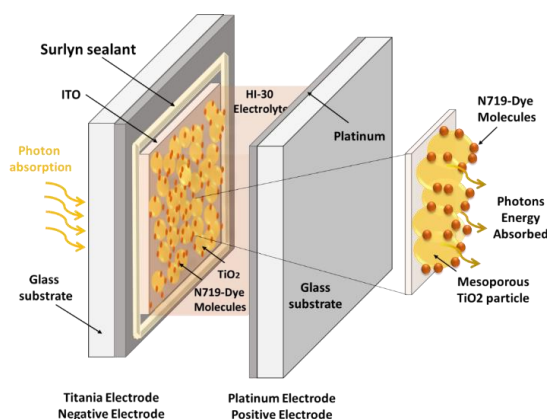


**Figure 1.** Schematic diagram of ITO/TiO<sub>2</sub>/N719-Dye/Pt electrode based electrochemical sensor.

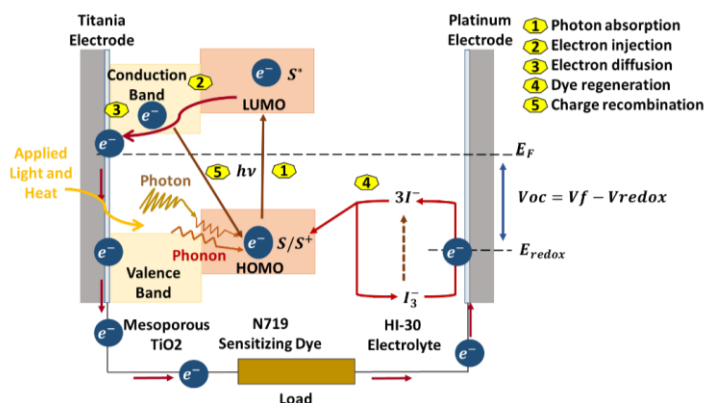


**Figure 2.** Working Principles of ITO/TiO<sub>2</sub>/N719-Dye/Pt electrode based electrochemical sensor

### 3. RESULTS AND DISCUSSION

Figure 3 shows the relationship between the photocurrent, voltage and irradiance. Both the  $V_{oc}$  and  $J_{sc}$  values increase when the light intensity gets higher. The linear increase in the photocurrent increases and voltages can be seen under varied light intensities. This linear relationship obeys the equation [15]:  $J_{sc} = C \times I^n$ . Where  $C$  is a constant,  $I$  is the light irradiance and  $n$  an exponent calculated from  $\text{Log}(J_{sc})$  Versus  $\text{Log}(I)$ . The value of the exponent  $n$  can be extracted from the relationship  $\text{Log}(J_{sc})$  versus  $\text{Log}(I)$ .

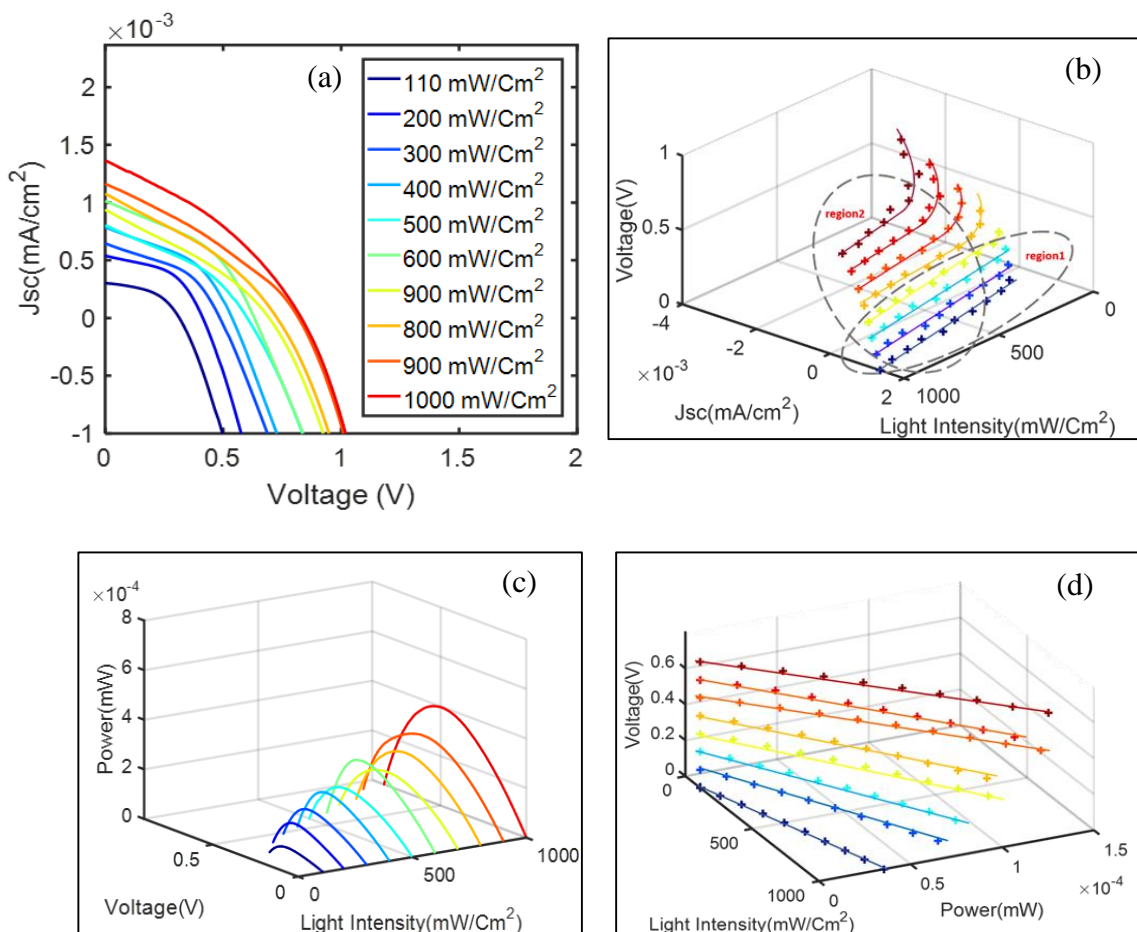


**Figure 3.** (a) I-V characteristic for ITO/TiO<sub>2</sub>/N719-Dye/Pt Electrode based electrochemical cells under varied irradiance variation, (b) photocurrent versus irradiance for different biasing voltages, (c) Output Power under irradiance variation and (d) Power versus irradiance variation for different biasing voltages

In Figure 3b, a deviation from linearity can be observed, for voltages above 0.3V under lower light intensities, the value of  $n$  has been calculated by considering the average from the calculated values for voltages 0-0.3 V. It has been found to be equal to 0.65. In fact, if the value of  $n$  is higher than 1 it implicates that there is a low density of the unoccupied trap states and if it is between 0.5 and 1, it lays in the case of the presence of continuous distribution of the trapping centers. In our case the value of  $n$  indicates the presence of continuous trapping centers distribution. The curves for short

circuit current density versus light irradiance presents a linear relationship for biasing voltages from 0V to 0.3V for all the applied light irradiance range, but a deviation from linearity has been observed only for the biasing voltages above 0.3V, and light irradiance below 400mW/Cm<sup>2</sup>. This means that the ideal operating region is either for low biasing voltage and all applied light irradiance (region1) or for all biasing voltages and high applied light irradiance (region2). The deviation illustrated in Figure 3 (b) is nothing but a drop in the  $J_{sc}$  current value. The illumination dependent variation of the power is displayed in 3(c), where the power increases proportionally with the increase of the light intensity. Figure 3 (d) clearly illustrates the linear relationship between the power and the light irradiance for all biasing voltages.

Response time  $t_r$  and recovery time  $t_c$  are important parameters to evaluate the photo-sensor performance.  $t_r$  and  $t_c$  are the time duration required for the photocurrent to reach the final high and low steady-state values respectively. The response speed determines how good is the device compared to the other reported sensors response speed. To determine the  $t_r$  and  $t_c$ , a discrete time on/off light pulses of 110mW cm<sup>-2</sup> and an average width of one second have been applied as displayed in Figure 4. The figure shows, when the device is excited with the light pulse, a small spike is generated indicating the generation of the two types of charge carriers. One of the charge carrier species produced recombination at the electrode, while the other species traveled through the active layer at a constant velocity, resulting in a slight plateau region in the transient curve. When the light is OFF, the number of electron-hole pairs generated slowly declined. The number of charge carriers generated upon illumination started to decrease. The second cycle showed relatively lower peak values and the subsequent transient cycles are almost identical with an average peak value of current ~0.11mA. The response time and recovery time have been calculated and found to be 0.22 sec and 0.63 sec respectively. The device response time is faster than when the recovery time, this can be explained by the fast photocurrent generation and the slow recombination that occurs inside the device. In fact, the number of excited dye molecules rapidly rises when the device is exposed to light, whereas, it responds steadily in the absence of light. This result can be validated in the coming section with the electrochemical impedance spectroscopy (EIS). The sensor's responsivity is determined by ( $R = I/AE$ ), where  $R$  the responsivity,  $I$  is the photocurrent value ( $2.35 \times 10^{-3}$  mA/Cm<sup>2</sup>),  $E$  is the irradiance of the source (110 mW/Cm<sup>2</sup>) and  $A$  is the effective area (0.072 cm<sup>2</sup>). When the sensor is used in photoconductive mode, the calculated responsivity is equal to  $3 \times 10^{-4}$  A/W, which is comparable and within the same range of other reported values from the literature [12, 13, 16, 17]. The photoconductive sensitivity of the device is calculated by  $S = (I_{sc} \times T)/(P \times A \times V)$ . Where  $T$  the thickness of the device,  $P$  the power of the incident light,  $A$  the active layer and  $V$  the applied biasing voltage. The photo-conductive sensitivity value was found to be equal to  $7 \mu\text{S.m.W}^{-1}$ .

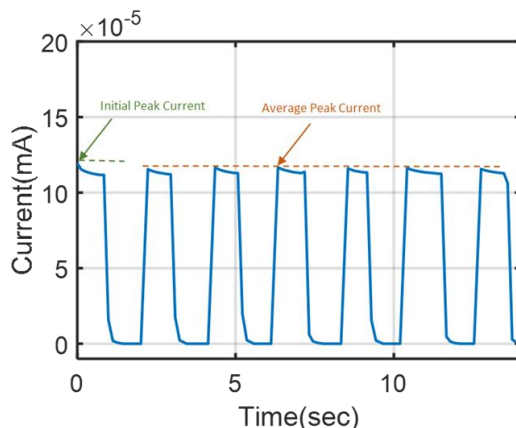


**Figure 4.** Transient response of the photo-sensor.

Figure 5 (a) exhibits a significant decrease in the generated photocurrent as a function of elevated temperature [18]. This is illustrated in both current density and output power linear decreasing function of the temperature as shown in Figure 5 (b). The sensor operating temperature range is from 30°C to 85°C for a certain applied voltage bias. These result are in agreement with earlier reported work [19]. Figure 5 (b) also illustrate the linear behavior of both short circuit current density and Output Power. The sensor sensitivity has been calculated to be 6  $\mu\text{A}\cdot\text{cm}^{-2}/^\circ\text{C}$ . These findings validate the possibility of using the electrochemical cell as a temperature sensor.

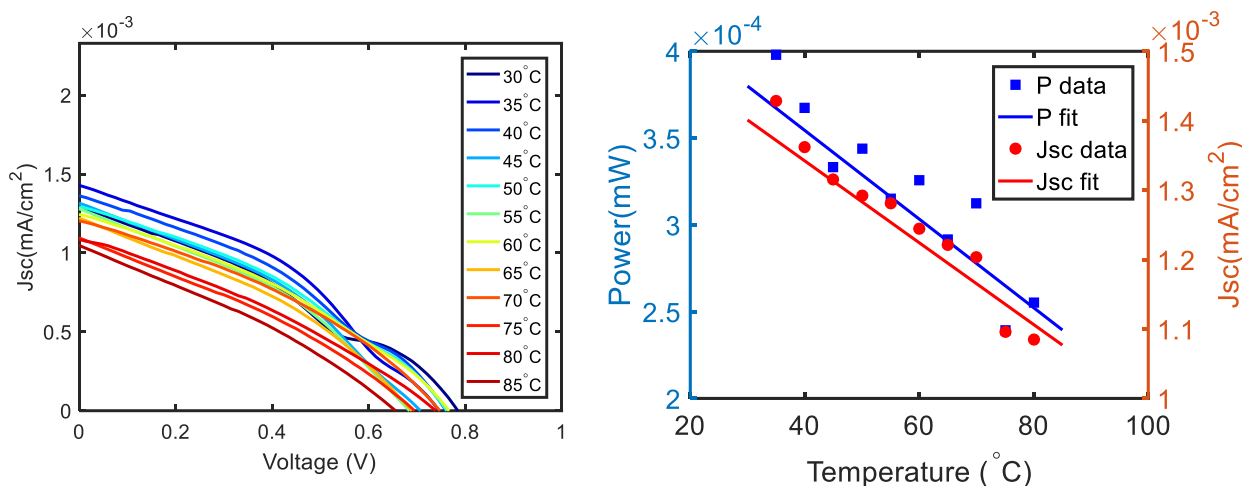


**Figure 5.** (a) I-V curves under temperature variation. (b) Power versus temperature and  $J_{sc}$  versus temperature graphs.

The Electrochemical Impedance spectroscopy (EIS) experiment has also been conducted under dark and light. The data has been used to plot the Nyquist plot under dark and light conditions as illustrated in Figure 6. The data has been fitted according to the model presented in Figure 7, which consists of a combination of series and parallel combination of resistors ‘R’ and Constant Phase Elements ‘CPE’. A goodness of fit of  $8.63 \times 10^{-4}$  for the light plot and  $3.98.7 \times 10^{-4}$  for the dark plot have been recorded. Typically, the Nyquist plot of a DSSC contains three semicircles. The first arc at the

high-frequency range attributed to the charge transfer process at the electrolyte /Pt interface. The second arc in the mid-frequency range representing the charge transfer process at the TiO<sub>2</sub>/dye/electrolyte interface. The third arc located in the low-frequency region represents the mass transport resistance of ions in the electrolyte. Since the high and low-frequency arcs are usually not easy to detect [20, 21], the EIS measures have been performed for several perturbation voltages 100, 300, 500, 600 and 700 mV. The best curve that slightly allows the detection of the high-frequency arc is for applied 300mV. Under light conditions, the diffusion component is not clearly distinguished in the high-frequency range, transport by diffusion and charge transport process is clear at the middle frequency range, while for lower frequency range, a low diffusion is recorded. For the dark Nyquist plot, we could distinguish the three main semicircles discussed above associated with additional RC arcs. The semicircles represent the electrons diffusion throughout the device. In fact, TiO<sub>2</sub> becomes very conductive and the transport resistance becomes negligible near the open circuit voltage [22]. Linking the EIS results to the findings discussed in the previous section, the photo-sensor response is expected to be highly related to the electron's diffusion rate across TiO<sub>2</sub> film and the limitations in ions diffusion in the electrolyte.

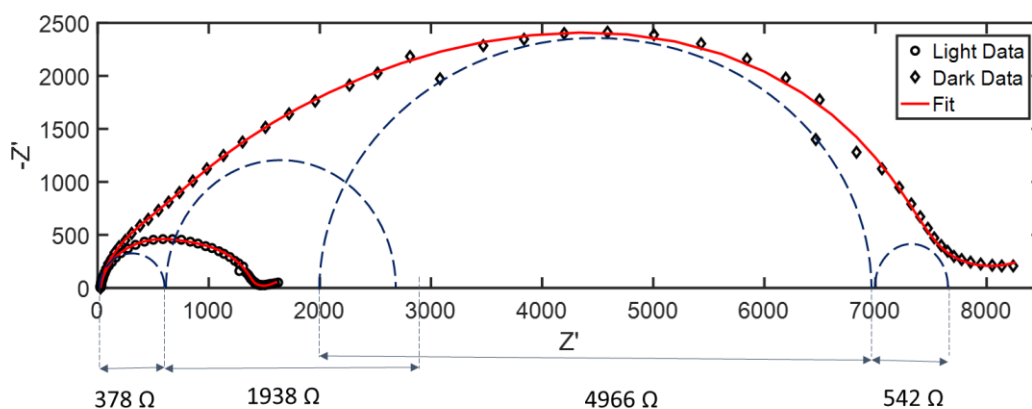


Figure 6. DSPE Nyquist plot under dark and light for 300mV biasing voltage

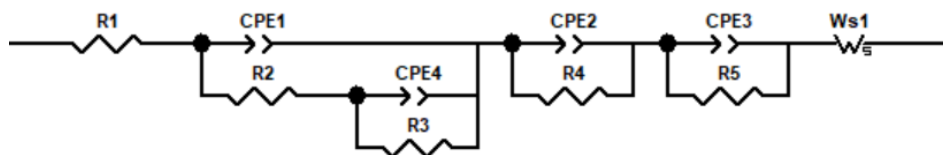


Figure 7. Equivalent Circuit to model the EIS data.

#### 4. CONCLUSION

Integrated light and temperature sensors were fabricated based on N719-dye. The performance of the fabricated sensors was investigated using I-V and electrochemical spectroscopy characterizations. The results showed that the sensors are quite sensitive to light and temperature

variation. The short-circuit current density increased linearly as a response to incremented light irradiance in the window of 110-1000mW/cm<sup>2</sup>. A deviation from linearity was recorded for biasing voltages above 0.3V. The experimental values measured for the sensor's responsivity, the response time, recovery time, and the photoconductive sensitivity were 3x10<sup>-4</sup> A/W, 220 msec, 630 msec, and 7 μS.m.W<sup>-1</sup>. These results are similar to those reported recently in the literature. Nevertheless, the sensor's spectral responsivity and sensitivity can be tuned by controlling the absorption spectrum of the photosensitive dye.

#### ACKNOWLEDGEMENT

The authors are thankful to the Center for Advanced Materials (CAM), Qatar University for its support to this work and to provide the experimental facilities to perform this work.

#### References

1. L. P. Lingwen Zeng, Dazhi Wu and Baoguo Yang, *Nutrition in Health and Disease - Our Challenges Now*, IntechOpen (2018) 313.
2. V. S. Manikandan, B. Adhikari and A. Chen, *Royal Society of chemistry*, 143 (2018) 4537.
3. A. Hagfeldt, U. B. Cappel, G. Boschloo, L. Sun, L. Kloo, H. Pettersson and E. A. Gibson, in *Practical Handbook of Photovoltaics* p. Elsevier (2012) 479.
4. M. Grätzel, *Journal of Photochemistry and Photobiology C: Photochemistry Reviews*, 4 (2003) 145.
5. J. MaçAira, L. Andrade and A. Mendes, *RSC Advances*, 4 (2014) 2830.
6. N. Tanabe, *Fujikura Technical Review*, 1 (2013) 109.
7. M. Shakeel, A. K. Pandey and N. Abd, *Renewable and Sustainable Energy Reviews*, 77 (2017) 89.
8. R. Su, S. Ashraf and A. El-Shafei, *Solar Energy*, 177 (2019) 724.
9. H. Al-Mumen, *Indian Journal of Science and Technology*, 10 (2017) 1.
10. C. T. C. Cesar, K. Sampei, O. Miho, O. Masataka and M. Norihisa, *Journal of Physics: Conference Series*, 557 (2014).
11. W. Wang, H. Yuan, Y. Zhang, J. Xie, D. Xu, X. Chen, Y. He, T. Zhang, Z. Chen and H. Shen, *Sensors and Actuators, A: Physical*, 275 (2018) 148.
12. A. S. Shikoh and Z. Ahmad, *RSC Advances* 7 (2017) 35445.
13. K. Wasman, Z. Ahmad, K. Sulaiman and C. Chin, *Synthetic Metals*, 210 (2015) 392.
14. A. M. Bagher, *International Journal of Renewable and Sustainable Energy* 3 (2014) 53.
15. A. Tataro, A. G. Al-sehemi, M. Özdemir, R. Özdemir and H. Usta, *ACS Appl. Mater. Interfaces* 519 (2017) 53.
16. A. S. Shikoh, Z. Ahmad, F. Touati, R. A. Shakoor and N. J. Al-thani, *RSC Advances* (2016) 53123.
17. A. Sephar, Z. Ahmad, F. Touati and S. A. Al-muhtaseb, *Optical Materials*, 78 (2018) 201.
18. S. R. Raga and F. Fabregat-Santiago, *Physical Chemistry Chemical Physics*, 15 (2013) 2328.
19. Z. Ahmad and R. A. Shakoor, *Applied Physics A*, 123 (2017) 1.
20. S. S. Negi, *ACS Omega*, 3 (2018) 1645.
21. D. Maheswari. P. Venkatachalam, *Acta Metall Sin* 28 (2015) 354.
22. L. Andrade, J. Sousa, H. Aguilar Ribeiro and A. Mendes, *Solar Energy*, 85 (2011) 781.